Progress In Electromagnetics Research C, Vol. 62, 157–165, 2016

Effects of Superstrate Layer on the Resonant Characteristics of Superconducting Rectangular Microstrip Patch Antenna

Sami Bedra[1, *] and Tarek Fortaki[2]

Abstract—The resonant characteristics of superconducting rectangular microstrip patch antenna with a superstrate layer are investigated using a full-wave spectral analysis in conjunction with the complex resistive boundary condition. The complex surface impedance of superconducting patch is determined using London's equation and the two-fluid model of Gorter and Casimir. Numerical results using the full-wave analysis presented here are in excellent agreement with theoretical and experimental results available in the open literature. Numerical results show that the effect of the superstrate layer on the resonant frequency and half-power bandwidth of the superconducting rectangular patch is stronger than that of the structure without superstrate layer as both the thickness and permittivity of the superstrate increase. Finally, numerical results concerning the effects of the parameters of superstrate-substrate and superconducting patch on the antenna performance are also presented and discussed.

1. INTRODUCTION

Microstrip patch antennas are a very important component of the communication systems and widely used as an efficient radiator due to their highly desirable attributes such as low profile structure, light weight, conformal shape, cost-effectiveness, high efficiency, ease of fixing, low volume, and compatibility with microwave integrated circuits (MIC), and : monolithic microwave integrated circuits (MMIC) are always sought in wireless systems [1–3]. However, they suffer from certain limitations such as narrow bandwidth and low gain. Due to recent development in wireless and mobile communications technologies, there exists a big demand of small antennas for applications such as mobile handsets, sensor networks, biomedical, wearable and Radio Frequency IDentification (RFID) systems [4]. These shortcomings have been investigated in detail by various researchers culminating in significant level of success [5].

In recent years, High-Temperature Superconductors (HTS) have given new dimensions to the industrial development of microwave circuits owing to their inductive properties also to their exceedingly small losses [6]. High Tc superconducting microstrip patch antennas have higher gain than their normal counterparts [7], due to the advantages of superconductors [8, 9]. Benefits of using high Tc superconducting materials at high frequencies include [8]: 1) very small losses, which means low attenuation and low noise level; 2) very low dispersion up to frequencies of several tens of GHz; 3) smaller devices due to minor losses, which leads to greater combination density; and 4) the transmission phase can be significantly reduced because of the smaller size and shorter interconnects [9], but they suffer from extremely narrow bandwidth, which severely limits their application [7].

There are many techniques [10–12] to enhance the bandwidth of conventional microstrip antennas. Bandwidth of antenna can be increased by designing the antenna with dielectric cover [13], where structures with substrate-superstrate are generally employed to improve the characteristics of the

Received 29 December 2015, Accepted 19 February 2016, Scheduled 3 March 2016

* Corresponding author: Sami Bedra (bedra_sami@hotmail.fr).

[1] Industrial Engineering Department, University of Khenchela, Khenchela 40004, Algeria. [2] Electronics Department, University of Batna, Batna 05000, Algeria.

resonator, especially those of the antenna [14]. Whether a superstrate over the patch is naturally formed or imposed by design may adversely affect the antenna's necessary performance characteristics such as resonant frequency, quality factor, bandwidth, radiation resistance, efficiency, and gain [15]. It has been presented that some of these methods are also efficient for High-Temperature Superconducting Microstrip antennas (HTSMAs) [16].

Several researchers have studied the effect of the air gap layer on the resonant frequency of high-Tc superconducting microstrip patch antenna [7, 10, 13, 17]. To the best of our knowledge, neither any design guideline nor any experimental or theoretical results are available in the open literature to predict the characteristics of high-Tc superconducting rectangular microstrip patch with substrate-superstrate configuration.

In [7], we studied the resonant characteristics behavior of covered high superconducting microstrip patch antennas using a full-wave spectral domain technique in conjunction with the compound resistive boundary condition. The effects of certain important parameters such as thickness and permittivity values of the superstrate and dielectric substrate, the dimensions and thickness of superconducting patch on the resonant frequencies are presented. Also, the impact of different parameters on the bandwidth of the antenna is also analyzed.

2. MATHEMATICAL FORMULATION

The high-Tc superconducting rectangular microstrip patch covered with the dielectric layer is shown in Figure 1.

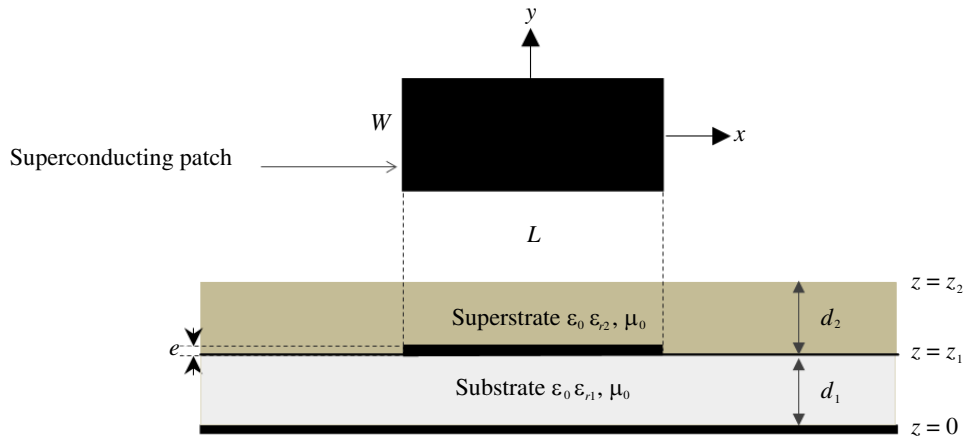

Figure 1. Geometrical structure of a superstrate-loaded of a high Tc superconducting rectangular microstrip patch antenna.

The rectangular superconducting patch of thickness e with dimensions (L, W) along the two axes (x, y), correspondingly, is printed on a grounded dielectric slab of thickness d_1. The substrate is characterized by the free-space permeability and a permittivity $\varepsilon_0\ \varepsilon_{r1}$. Overhead the radiating patch a superstrate layer of thickness d_2 with permeability μ_0 and permittivity $\varepsilon_0\ \varepsilon_{r2}$. The ambient medium is air with constitutive parameters and ε_0. All fields and currents are harmonic time with time dependence suppressed. The transverse fields inside the jth layer ($j = 1, 2$) can be obtained via the inverse vector Fourier transforms as shown in [13]

$$\mathbf{E}(\mathbf{r}_s, z) = \begin{bmatrix} E_x(\mathbf{r}_s, z) \\ E_y(\mathbf{r}_s, z) \end{bmatrix} = \frac{1}{4\pi^2} \int_{-\infty}^{+\infty} \int_{-\infty}^{+\infty} \overline{\mathbf{F}}(\mathbf{k}_s, \mathbf{r}_s) \cdot \mathbf{e}(\mathbf{k}_s, z) dk_x dk_y \tag{1}$$

$$\mathbf{H}(\mathbf{r}_s, z) = \begin{bmatrix} H_y(\mathbf{r}_s, z) \\ -H_x(\mathbf{r}_s, z) \end{bmatrix} = \frac{1}{4\pi^2} \int_{-\infty}^{+\infty} \int_{-\infty}^{+\infty} \overline{\mathbf{F}}(\mathbf{k}_s, \mathbf{r}_s) \cdot \mathbf{h}(\mathbf{k}_s, z) dk_x dk_y \tag{2}$$

where $\overline{\mathbf{F}}(\mathbf{k}_s, \mathbf{r}_s) = \frac{1}{k_s}\begin{bmatrix} k_x & k_y \\ k_y & -k_x \end{bmatrix} \mathbf{e}^{\mathrm{i}k_s \cdot r_s}$ is the kernel of the vector Fourier transform [18], and the continuity equations for the tangential field components are

$$\mathbf{e}(\mathbf{k}_s, z_j^-) = \mathbf{e}(\mathbf{k}_s, z_j^+) = \mathbf{e}(\mathbf{k}_s, z_j), \quad j = 1, 2 \tag{3}$$

$$\mathbf{h}(\mathbf{k}_s, z_j^-) - \mathbf{h}(\mathbf{k}_s, z_j^+) = \delta_{j1}\mathbf{j}(\mathbf{k}_s), \quad j = 1, 2 \tag{4}$$

$\mathbf{j}(\mathbf{k}_s)$ in Eq. (4) is the vector Fourier transform of the current on the superconducting patch $\mathbf{J}(\mathbf{r}_s)$ and accounts for the discontinuity of the tangential magnetic field at the interface $z = d_1$, and δ_{j1} is the Kronecker symbol [18].

The transverse electric field must necessarily be nil on a perfect conductor so that for the ground plane we have [13]

$$\mathbf{e}(\mathbf{k}_s, 0^-) = \mathbf{e}(\mathbf{k}_s, 0^+) = \mathbf{e}(\mathbf{k}_s, 0) = \mathbf{0} \tag{5}$$

In the unbounded air area above the superstrate of the considered structure ($d_1 + d_2 < z < +\infty$ and $\varepsilon_r = 1$), the electromagnetic field given by Eqs. (6) and (7) should vanish at $z \to +\infty$ according to Sommerfeld's condition of radiation. This yields

$$\mathbf{h}\left(\mathbf{k}_s, (d_1 + d_2)^+\right) = \overline{\mathbf{g}}_0(\mathbf{k}_s) \cdot \mathbf{e}\left(\mathbf{k}_s, (d_1 + d_2)^+\right) \tag{6}$$

From Eqs. (4)–(6), we obtain a relation among $\mathbf{j}(\mathbf{k}_s)$ and $\mathbf{e}(\mathbf{k}_s, d_1)$ given by

$$\mathbf{e}(\mathbf{k}_s, d_1) = \overline{\mathbf{G}}(\mathbf{k}_s) \cdot \mathbf{j}(\mathbf{k}_s) \tag{7}$$

where $\overline{\mathbf{G}}(\mathbf{k}_s)$ is the dyadic Green's function in the Vector Fourier transform domain, and it is given by [13]

$$\overline{\mathbf{G}}(\mathbf{k}_s) = \begin{bmatrix} G11 & 0 \\ 0 & G22 \end{bmatrix} = \left[\overline{\mathbf{T}}_1^{22} \cdot \left(\overline{\mathbf{T}}_1^{12}\right)^{-1} + \left(\overline{\mathbf{g}}_0 \cdot \overline{\mathbf{T}}_2^{12} - \overline{\mathbf{T}}_2^{22}\right)^{-1} \cdot \left(\overline{\mathbf{g}}_0 \cdot \overline{\mathbf{T}}_2^{11} - \overline{\mathbf{T}}_2^{21}\right)\right]^{-1} \tag{8}$$

In the vector Fourier transform domain, the transverse electric field at the plane of the rectangular superconducting patch can be written by the way of a superposition of an electric field in the patch and another out of the patch, and this yields [8]

$$\mathbf{e}(\mathbf{k}_s, d) = \mathbf{e}^i(\mathbf{k}_s, d) + \mathbf{e}^o(k_s, d) \tag{9}$$

The electric field in the rectangular superconducting patch is given by

$$\mathbf{e}^i(\mathbf{k}_s, d) = Z_s \cdot \mathbf{j}(\mathbf{k}_s) \tag{10}$$

where Z_s is the surface impedance of the superconducting patch. When the thickness of the superconducting patch is less than three times of the zero-temperature penetration depth (λ_0), Z_s can be expressed as follows [16–19]:

$$Z_s = \frac{1}{e\sigma} \tag{11}$$

where Z_s is the complex conductivity of the superconducting film. It is determined by using London's equation and the Gorter-Casimir two-fluid model as [16–19]

$$\sigma = \sigma_n \left(\frac{T}{T_c}\right)^4 - \mathrm{i}\frac{1 - \left(\dfrac{T}{T_c}\right)^4}{\omega\mu_0\lambda_0^2} \tag{12}$$

where T is the temperature, T_c the transition temperature, σ_n the normal state conductivity at $T = T_c$ and ω the angular frequency. Substituting Eq. (9) in Eq. (7) and using Eq. (10) yields

$$\mathbf{e}^o(\mathbf{k}_s, d) = \left[\overline{\mathbf{G}}(k_s) - Z_s\overline{\mathbf{I}}\right] \cdot \mathbf{j}(\mathbf{k}_s) \tag{13}$$

where $\overline{I}$ stands for the 2×2 unit matrix. The transverse electric field out of the patch can be obtained from Eq. (13) via the inverse vector Fourier transform as follows:

$$\mathbf{E}^o(\mathbf{r}_s, d) = \frac{1}{4\pi^2} \int_{-\infty}^{+\infty} \int_{-\infty}^{+\infty} \overline{\mathbf{F}}(\mathbf{k}_s, \mathbf{r}_s) \cdot \left[\overline{\mathbf{G}}(\mathbf{k}_s) - Z_s\overline{\mathbf{I}}\right] \cdot \mathbf{j}(\mathbf{k}_s) dk_x dk_y \tag{14}$$

Implementation of the boundary condition requiring the transverse electric field of Eq. (14) to vanish on the area of the superconducting patch yields the sought integral equation

$$\int_{-\infty}^{+\infty}\int_{-\infty}^{+\infty} \overline{\mathbf{F}}(\mathbf{k}_s,\mathbf{r}_s)\cdot\left[\,\overline{\mathbf{G}}(\mathbf{k}_s)-Z_s\bar{\mathbf{I}}\,\right]\cdot\mathbf{j}(\mathbf{k}_s)dk_xdk_y=\mathbf{0},\quad (x,y)\in\text{patch} \tag{15}$$

The first step in the Galerkin's method solution of Eq. (15) is to expand the patch current $\mathbf{J}(\mathbf{r}_s)$ into a finite series of known basis functions J_{xn} and J_{ym}

$$\mathbf{J}(\mathbf{r}_s)=\sum_{n=1}^{N}a_n\begin{bmatrix} J_{xn}(\mathbf{r}_s)\\ 0\end{bmatrix}+\sum_{m=1}^{M}b_m\begin{bmatrix} 0\\ J_{ym}(\mathbf{r}_s)\end{bmatrix} \tag{16}$$

where a_n and b_m are the mode expansion coefficients to be sought. The resulting equation from substituting the vector Fourier transform of Eq. (16) into Eq. (15) is tested by the same set of basis functions used in the expansion of the patch current. Thus, the integral equation Eq. (15) is reduced to a system of linear equations which can be written compactly in matrix form as [18]

$$\begin{bmatrix} \left(\overline{\mathbf{Z}}^{11}\right)_{N\times N} & \left(\overline{\mathbf{Z}}^{12}\right)_{N\times M}\\ \left(\overline{\mathbf{Z}}^{21}\right)_{M\times N} & \left(\overline{\mathbf{Z}}^{22}\right)_{M\times M}\end{bmatrix}\cdot\begin{bmatrix}(\mathbf{a})_{N\times 1}\\ (\mathbf{b})_{M\times 1}\end{bmatrix}=0 \tag{17}$$

where the components of the impedance matrix $(\overline{\mathbf{Z}})_{(N+M)\times(N+M)}$ are given by

$$\left(\overline{\mathbf{Z}}^{11}\right)_{kn}=\int_{-\infty}^{+\infty}\int_{-\infty}^{+\infty}\frac{1}{k_s^2}\left[k_x^2G11+k_y^2G22-k_s^2Z_s\right]\tilde{J}_{xk}(-\mathbf{k}_s)\tilde{J}_{xn}(\mathbf{k}_s)dk_xdk_y \tag{18a}$$

$$\left(\overline{\mathbf{Z}}^{12}\right)_{km}=\int_{-\infty}^{+\infty}\int_{-\infty}^{+\infty}\frac{k_xk_y}{k_s^2}[G11-G22]\tilde{J}_{xk}(-\mathbf{k}_s)\tilde{J}_{ym}(\mathbf{k}_s)dk_xdk_y \tag{18b}$$

$$\left(\overline{\mathbf{Z}}^{21}\right)_{ln}=\int_{-\infty}^{+\infty}\int_{-\infty}^{+\infty}\frac{k_xk_y}{k_s^2}[G11-G22]\tilde{J}_{yl}(-\mathbf{k}_s)\tilde{J}_{xn}(\mathbf{k}_s)dk_xdk_y \tag{18c}$$

$$\left(\overline{\mathbf{Z}}^{22}\right)_{lm}=\int_{-\infty}^{+\infty}\int_{-\infty}^{+\infty}\frac{1}{k_s^2}\left[k_y^2G11+k_x^2G22-k_s^2Z_s\right]\tilde{J}_{yl}(-\mathbf{k}_s)\tilde{J}_{ym}(\mathbf{k}_s)dk_xdk_y \tag{18d}$$

In Eqs. (16)–(18), $\tilde{J}_{xn}$ and $\tilde{J}_{ym}$ are the scalar Fourier transforms of J_{xn} and J_{ym}, respectively. For the existence of a non-trivial solution of Eq. (17), we must have

$$\det\left[\overline{\mathbf{Z}}(\omega)\right]=0 \tag{19}$$

Eq. (19) is an eigenequation for ω, from which the characteristics of the structure of Figure 1 can be obtained. In fact, let $\omega=2\pi(f_r+\mathrm{i}f_i)$ be the complex root of Eq. (19). In that case, the quantity f_r stands for the resonant frequency; the quantity $\mathrm{BW}=2f_i/f_r$ stands for the half-power bandwidth; the quantity $Q=f_r/(2f_i)$ stands for the quality factor.

3. NUMERICAL RESULTS AND DISCUSSION

In order to check the correctness of our formulation described in the previous section, two cases are considered. The first concerns the rectangular microstrip patch, and the calculated results of resonant frequencies and half power bandwidth are compared with the published experimental data [20]. Table 1 summarizes the measured and computed resonant frequencies and bandwidths for different geometrical antennas.

Table 1. Comparison of the calculated resonant frequency and half-power bandwidth with experimental data, for a superstrate-loaded rectangular patch, $W = 19\,\text{mm}$, $L = 22.9\,\text{mm}$, $d_1 = 1.59\,\text{mm}$, $\varepsilon_{r1} = 2.32$.

Input parameters			Resonant frequencies [GHz]		Bandwidth (%)	
Dielectric cover	ε_{r2}	d_2 (mm)	Measured [20]	This paper	Measured [20]	This paper
Air	1.0	∞	4.104	4.123	2.17	2.75
Duroid	2.32	0.8	4.008	4.033	2.18	2.70
		1.59	3.934	3.983	2.22	2.75
		3.18	3.895	3.924	2.31	2.96
Plexiglass	2.6	1.12	3.952	3.991	2.18	2.71
		1.59	3.912	3.958	2.18	2.74
		3.18	3.874	3.887	2.20	2.98
		6.36	3.806	3.822	2.32	3.93
Mylar	3.0	0.064	4.070	4.108	2.18	2.73
		0.128	4.058	4.095	2.18	2.72
		0.384	4.010	4.051	2.20	2.69
Epsilam-10	10.2	0.635	3.640	3.782	2.0	2.49
Custom High-K	10	1.54	3.482	3.518	1.75	2.53
		3.12	3.26	3.222	1.90	3.13

As the second case, we compare our theoretically computed values of resonant frequencies by using the method described in Section 2, with previous theoretical results [21], of superconducting rectangular patch for three different lengths (L). The rectangular superconducting patch is fabricated with a YBCO ($YB_{a2}C_{u3}O_x$) was assumed to be $e = 350\,\text{nm}$ thick with very good quality and a critical temperature $T_c = 89\,\text{K}$, zero-temperature penetration depth $\lambda_0 = 140\,\text{nm}$, and normal state conductivity $\sigma_n = 1\,\text{S/m}$. The operating temperature is $T = 77\,\text{K}$. Table 2 summarizes the calculated resonance frequencies and those obtained through the cavity model [21] for three different lengths of the patch, and less than 2% differences between these results are obtained.

Table 2. Comparison of calculated resonant frequencies with those presented by Richard et al. [21]; $W = 1630\,\mu\text{m}$, $\sigma_n = 10^6\,\text{S/m}$, $T_c = 89\,\text{K}$, $\lambda_0 = 140\,\text{nm}$, $e = 350\,\text{nm}$, $T = 77\,\text{K}$, $\varepsilon_r = 23.81$, $d = 254\,\mu\text{m}$.

L (μm)	**Resonant Frequency (GHz)**		**Errors (%)**
	Cavity Model [21]	**Present study**	
935	28.95	28.76	0.66
1050	26.12	26.29	0.65
1100	25.05	25.33	1.12

Figure 2 shows the variations of the resonant characteristics as function of the thickness e of the superconducting rectangular microstrip patch. Figure 2(a) presents the dependence of the resonant frequency on the thickness of the superconducting patch with different thicknesses of the superstrate layer. The bandwidth of the superconducting patch antenna against the thickness of the superconducting patch for different superstrates is shown in Figure 2(b). The superconducting materials YBCO of very good quality have a critical temperature $T_c = 89\,\text{K}$, zero-temperature penetration depth $\lambda_0 = 140\,\text{nm}$, and normal state conductivity $\sigma_n = 10^6\,\text{S/m}$. The operating temperature is $T = 44.5\,\text{K}$. The dimension of the rectangular patch is $W \times L = 30\,\text{mm} \times 20\,\text{mm}$. The substrate is chosen to be $\varepsilon_{r1} = 2.33$ with thickness $d_1 = 1.4\,\text{mm}$ and the superstrate layer with $\varepsilon_{r2} = 5$.

From Figures 2(a) and 2(b), it can be observed that the resonant frequency and bandwidth increase quickly with increasing superconducting film thickness e until a value of $e = \lambda_0$, and beyond this value, the resonant frequency and bandwidth are insensitive to the increasing of e. It is also observed that the resonant frequency shifts to higher values in the case of low value of thickness of the superstrate layer and smaller in the case of the high values of the thicknesses. Therefore, the effect of a protected layer is more

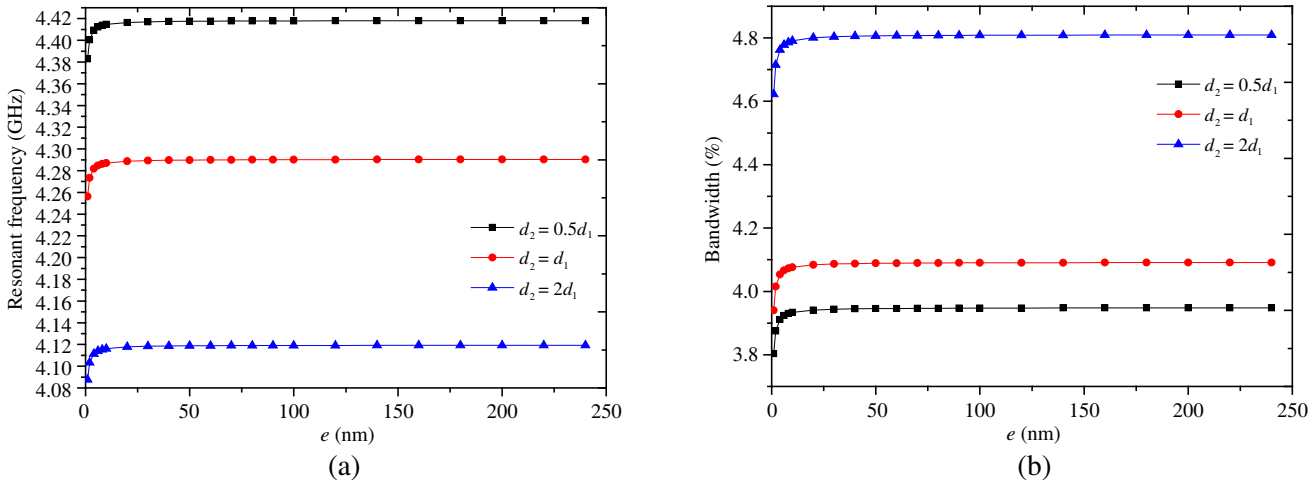

Figure 2. (a) Resonant frequency, and (b) bandwidth of the high T_c superconducting microstrip patch with different thicknesses of superstrate layer against the thickness of patch; $\sigma_n = 10^6$ S/m, $\lambda_0 = 140$ nm, $T/T_c = 0.5$, $W = 30$ mm, $L = 20$ mm, $\varepsilon_{r1} = 2.33$, $d_1 = 1.4$ mm, $\varepsilon_{r2} = 5$.

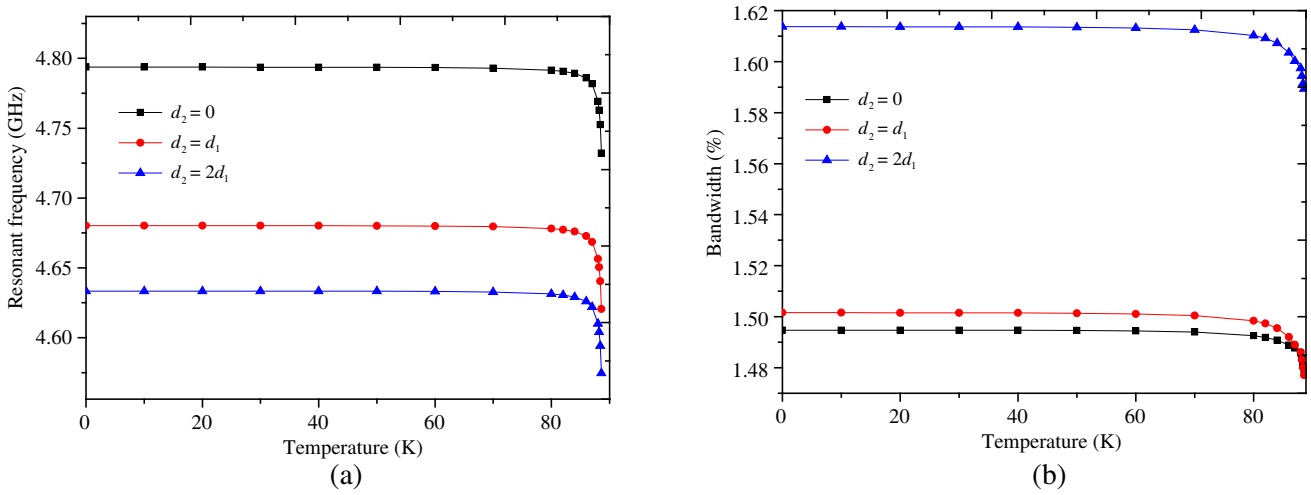

Figure 3. (a) Resonant frequency, and (b) bandwidth of the high T_c superconducting microstrip patch with different thicknesses of superstrate layer against operating temperature; $\sigma_n = 10^6$ S/m, $\lambda_0 = 180$ nm, $T_c = 89$ K, $e = 140$ nm, $W = 30$ mm, $L = 20$ mm, $\varepsilon_{r1} = \varepsilon_{r2} = 2.2$, $d_1 = 0.5$ mm.

pronounced for a thick superstrate than for a thin superstrate. This is accredited to the fact that for thick superstrate, in addition, the half power bandwidth of superconducting microstrip antenna increases with increased thickness of the superstrate layer. Thus it can be concluded that the introduction of the superstrate layer enhances the half-power bandwidth of a superconducting rectangular microstrip patch antenna, and this enhancement is more pronounced for superconducting patches having higher thicknesses.

The influence of the operating temperature on the resonant characteristics of superconducting rectangular microstrip patch with different thicknesses of superstrate layer is investigate in Figure 3. The superconducting patch of dimension $W \times L = 30\,\text{mm} \times 20\,\text{mm}$ is made of an $e = 140$ nm thick YBCO thin rectangular film with a normal state conductivity at the transition temperature $\sigma_n = 10^6$ S/m, zero-temperature penetration depth $\lambda_0 = 180$ nm and transition temperature $T_c = 89$ K. The substrate is chosen to be $\varepsilon_{r1} = 2.2$ with thickness $d_1 = 1.4$ mm and the superstrate layer with dielectric permittivity $\varepsilon_{r2} = 2.2$. The resonant frequency and half-power bandwidth of the superconducting microstrip antenna against operating temperature for three different thicknesses of superstrate layer are shown

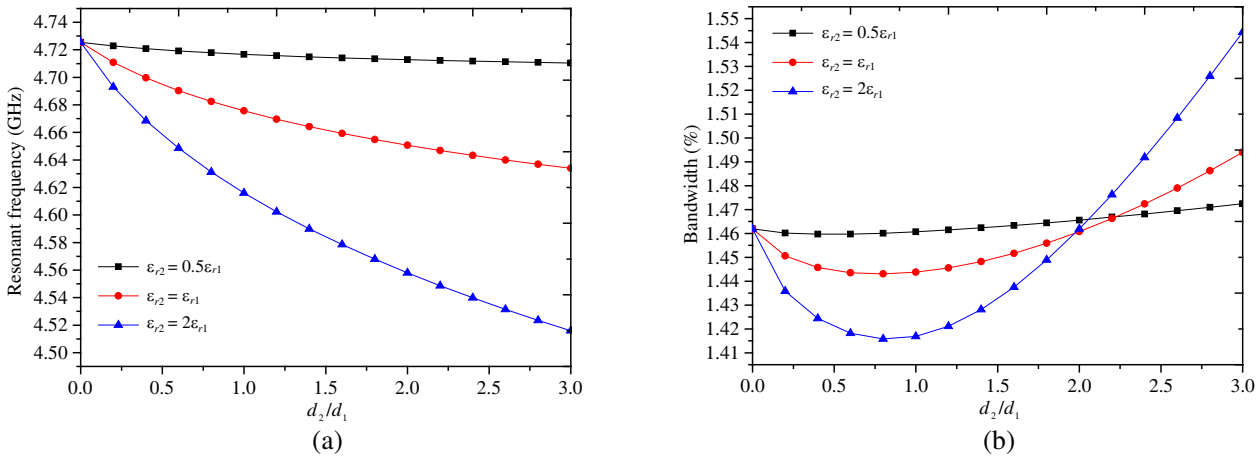

Figure 4. (a) Resonant frequencies and (b) half-power bandwidth of high T_c superconducting microstrip antenna with different permittivities of a superstrate layer versus the superstrate thickness; $\varepsilon_{r1} = 2.4$, $d_1 = 0.508\,\text{mm}$, $W = 30\,\text{mm}$, $L = 20\,\text{mm}$, $\sigma_n = 10^6\,\text{S/m}$, $\lambda_0 = 180\,\text{nm}$, $e = 140\,\text{nm}$, $T/T_c = 0.5$.

in Figures 4(a) and 4(b), respectively. It is observed that the effect of varying the temperature on the resonant frequency and bandwidth is significant only for temperatures near the transition temperature. Note that the steep change in the resonant frequency and bandwidth at temperatures near Tc can be attributed to a change in the magnetic penetration depth of the YBCO [18].

The resonant characteristics of superconducting rectangular microstrip antenna as a function of superstrate thickness are shown in Figure 4. The dimension of the rectangular patch is $W \times L = 30\,\text{mm} \times 20\,\text{mm}$. The superconducting material characteristics are $\sigma_n = 10^6\,\text{S/m}$, $e = 140\,\text{nm}$, $T/T_c = 0.5$, and $\lambda_0 = 180\,\text{nm}$. The substrate is chosen to be $\varepsilon_{r1} = 2.4$ with thickness $d_1 = 0.508\,\text{mm}$. The results are presented for the resonant frequency and half-power bandwidth of superstrate loaded superconducting rectangular patch against the thickness and different permittivities of the superstrate layer. The resonant frequencies of the structures with a superstrate layer are smaller than that of the structure without a superstrate since the effective permittivity of the medium surrounding the superconducting patch is higher in the former case than in the latter one. Also, the bandwidth of the structure without a superstrate layer tends to be narrower than that of the structure with a superstrate since the fringing field and radiation are most pronounced in the first case than in the second case. Note that these results agree with those discovered theoretically for perfectly conducting rectangular patch [22]. The effect of the superstrate layer on the resonant frequency and half-power bandwidth of the superconducting rectangular patch is stronger than that of the structure without superstrate layer as both the thickness and permittivity of the superstrate increase.

4. CONCLUSION

This work presents the resonant characteristics of superstrate loaded superconducting rectangular microstrip patch antenna. The analysis has been based on a full-wave model with London's equations and the Gorter-Casimir two-fluid model. Numerical results concerning the effect of a superconductor patch on the resonant characteristics of the antenna are presented. These results have shown that the influence of the operating temperature on the resonant frequencies and bandwidth of superstrate loaded superconducting rectangular microstrip patch antenna is especially significant for temperatures near the transition temperature. Further results show that as the thickness of superconductor patch grows, the resonant frequency (bandwidth) increases quickly until the thickness of patch reaches penetration depth. The obtained results also indicate that the effect of the superstrate layer on the resonant characteristics of the superconducting patch is stronger for higher superstrate thickness and permittivity. The accuracy of our results has been checked with different approaches and shows a very good agreement. Thus, superconducting patch in substrate superstrate configuration could give wide bandwidth with high gain by proper selection of superstrate thickness and its dielectric constants.

REFERENCES

1. Maity, S. and B. Gupta, "Cavity model analysis of 30°–60°–90° triangular microstrip antenna," *AEU-International Journal of Electronics and Communications*, Vol. 69, 923–932, 2015.
2. Singh, A., R. K. Gangwar, and B. K. Kanaujia, "Cavity backed annular ring microstrip antenna loaded with concentric circular patch," *8th European Conference onAntennas and Propagation (EuCAP), 2014*, 2155–2158, 2014.
3. Khanna, A., D. K. Srivastava, and J. P. Saini, "Bandwidth enhancement of modified square fractal microstrip patch antenna using gap-coupling," *Engineering Science and Technology*, Vol. 18, 286–293, 2015.
4. Raval, F., Y. Kosta, and H. Joshi, "Reduced size patch antenna using complementary split ring resonator as defected ground plane," *AEU-International Journal of Electronics and Communications*, Vol. 69, 1126–1133, 2015.
5. Khan, Q. U. and M. B. Ihsan, "Higher order mode excitation for high gain microstrip patch antenna," *AEU-International Journal of Electronics and Communications*, Vol. 68, 1073–1077, 2014.
6. Lamine Tounsi, M. and M. C. Yagoub, "Efficient characterization of EMC shielding in anisotropic high-Tc superconducting devices for industrial applications," *International Journal of RF and Microwave Computer-Aided Engineering*, Vol. 22, 116–123, 2012.
7. Benkouda, S., M. Amir, T. Fortaki, and A. Benghalia, "Dual-frequency behavior of stacked high Tc superconducting microstrip patches," *Journal of Infrared, Millimeter, and Terahertz Waves*, Vol. 32, 1350–1366, 2011.
8. Fortaki, T., A. Mounir, S. Benkouda, and A. Benghalia, "Study of high Tc superconducting microstrip antenna," *PIERS Online*, Vol. 5, No. 4, 346–349, 2009.
9. El-Ghazaly, S. M., R. B. Hammond, and T. Itoh, "Analysis of superconducting microwave structures: Application to microstrip lines," *IEEE Transactions on Microwave Theory and Techniques*, Vol. 40, 499–508, 1992.
10. Benmeddour, F., C. Dumond, F. Benabdelaziz, and F. Bouttout, "Improving the performances of a high Tc superconducting circuslar microstrip antenna with multilayered configuration and anisotropic dielectrics," *Progress In Electromagnetics Research C*, Vol. 18, 169–183, 2011.
11. Chebbara, F., S. Benkouda, and T. Fortaki, "Fourier transform domain analysis of high Tc superconducting rectangular microstrip patch over ground plane with rectangular aperture," *Journal of Infrared, Millimeter, and Terahertz Waves*, Vol. 31, 821–832, 2010.
12. Bedra, S., T. Fortaki, A. Messai, and R. Bedra, "Spectral domain analysis of resonant characteristics of high Tc superconducting rectangular microstrip patch printed on isotropic or uniaxial anisotropic substrates," *Wireless Personal Communications*, Vol. 86, 495–511, 2016.
13. Fortaki, T., L. Djouane, F. Chebara, and A. Benghalia, "Radiation of a rectangular microstrip patch antenna covered with a dielectric layer," *International Journal of Electronics*, Vol. 95, 989–998, 2008.
14. Zebiri, C., M. Lashab, and F. Benabdelaziz, "Asymmetrical effects of bi-anisotropic substrate-superstrate sandwich structure on patch resonator," *Progress In Electromagnetics Research B*, Vol. 49, 319–337, 2013.
15. Biswas, M. and A. Mandal, "Experimental and theoretical investigation of resonance and radiation characteristics of superstrate loaded rectangular patch antenna," *Microwave and Optical Technology Letters*, Vol. 57, 791–799, 2015.
16. Barkat, O. and A. Benghalia, "Radiation and resonant frequency of superconducting annular ring microstrip antenna on uniaxial anisotropic media," *Journal of Infrared, Millimeter, and Terahertz Waves*, Vol. 30, 1053–1066, 2009.
17. Bedra, S. and T. Fortaki, "Hankel transform domain analysis of covered circular microstrip patch printed on an anisotropic dielectric layer," *Journal of Computational Electronics*, Vol. 14, 747–753, 2015.

18. Benkouda, S., A. Messai, M. Amir, S. Bedra, and T. Fortaki, "Characteristics of a high Tc superconducting rectangular microstrip patch on uniaxially anisotropic substrate," *Physica C: Superconductivity*, Vol. 502, 70–75, 2014.
19. Da Silva, S., A. d'Assuncao, and J. Oliveira, "Analysis of high Tc superconducting microstrip antennas and arrays," *International Conference in Microwave and Optoelectronics 1999, SBMO/IEEE MTT-S, APS and LEOS-IMOC'99*, 243–246, 1999.
20. Bahl, I. J., P. Bhartia, and S. S. Stuchly, "Design of microstrip antennas covered with a dielectric layer," *IEEE Transactions on Antennas and Propagation*, Vol. 30, 314–318, 1982.
21. Richard, M. A., K. B. Bhasin, and P. C. Claspy, "Superconducting microstrip antennas: An experimental comparison of two feeding methods," *IEEE Transactions on Antennas and Propagation*, Vol. 41, 967–974, 1993.
22. Bouttout, F., F. Benabdelaziz, T. Fortaki, and D. Khedrouche, "Resonant frequency and bandwidth of a superstrate-loaded rectangular patch on a uniaxial anisotropic substrate," *Communications in Numerical Methods in Engineering*, Vol. 16, 459–473, 2000.